Tip induced mechanical deformation of epitaxial graphene grown on reconstructed 6H–SiC(0001) surface during scanning tunneling and atomic force microscopy studies

José A. Morán-Meza, Christophe Lubin, François Thoyer, Jacques Cousty

Tip induced mechanical deformation of epitaxial graphene grown on reconstructed 6H–SiC(0001) surface during scanning tunneling and atomic force microscopy studies

2015 Nanotechnology 26 255704

(http://iopscience.iop.org/0957-4484/26/25/255704)

IOP Publishing Nanotechnology
Nanotechnology **26** (2015) 255704 (7pp) doi:10.1088/0957-4484/26/25/255704

Tip induced mechanical deformation of epitaxial graphene grown on reconstructed 6H–SiC(0001) surface during scanning tunneling and atomic force microscopy studies

José Antonio Morán Meza[1,2,3], Christophe Lubin[1], François Thoyer[1] and Jacques Cousty[1]

[1] Service de Physique de l'Etat Condensé, DSM/IRAMIS/SPEC, CNRS UMR 3680, CEA Saclay, F-91191 Gif sur Yvette Cedex, France
[2] Grupo de Materiales Nanoestructurados, Facultad de Ciencias, Universidad Nacional de Ingeniería, Av. Túpac Amaru 210, Lima 25, Peru

E-mail: jmoranm@uni.edu.pe, christophe.lubin@cea.fr, francois.thoyer@cea.fr and jacques.cousty@cea.fr

Received 24 February 2015, revised 6 April 2015
Accepted for publication 17 April 2015
Published 4 June 2015

Abstract

The structural and mechanical properties of an epitaxial graphene (EG) monolayer thermally grown on top of a 6H–SiC(0001) surface were studied by combined dynamic scanning tunneling microscopy (STM) and frequency modulation atomic force microscopy (FM-AFM). Experimental STM, dynamic STM and AFM images of EG on 6H–SiC(0001) show a lattice with a 1.9 nm period corresponding to the (6 × 6) quasi-cell of the SiC surface. The corrugation amplitude of this (6 × 6) quasi-cell, measured from AFM topographies, increases with the setpoint value of the frequency shift Δf (15–20 Hz, repulsive interaction). Excitation variations map obtained simultaneously with the AFM topography shows that larger dissipation values are measured in between the topographical bumps of the (6 × 6) quasi-cell. These results demonstrate that the AFM tip deforms the graphene monolayer. During recording in dynamic STM mode, a frequency shift (Δf) map is obtained in which Δf values range from 41 to 47 Hz (repulsive interaction). As a result, we deduced that the STM tip, also, provokes local mechanical distortions of the graphene monolayer. The origin of these tip-induced distortions is discussed in terms of electronic and mechanical properties of EG on 6H–SiC(0001).

Keywords: epitaxial graphene, STM, AFM, mechanical properties, silicon carbide

(Some figures may appear in colour only in the online journal)

1. Introduction

Graphene, a single layer of sp^2-bonded carbon atoms arranged in a two-dimensional honeycomb lattice, has attracted considerable attention due to potential applications in many technological domains [1]. Mechanical exfoliation [1], chemical vapor deposition of hydrocarbons on different metal surfaces [2] and thermal decomposition of commercial SiC crystals [3] are the main roads to synthesize graphene. The latter technique which yields epitaxial graphene (EG) grown on the 6H–SiC(0001) surface is considered particularly a promising method for the production of large graphene areas suitable for electronic device applications. The structure of graphene covering a 6H–SiC(0001) surface (the Si-face of silicon carbide) has been intensively investigated mainly by low energy electron diffraction and scanning tunneling

[3] Author to whom any correspondence should be addressed.

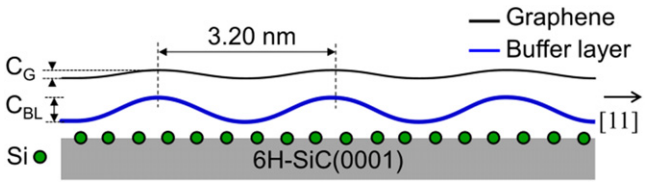

Figure 1. Side view of the structure of graphene grown on top of a 6H–SiC(0001) surface along the [11] direction of the (6 × 6) quasi-cell.

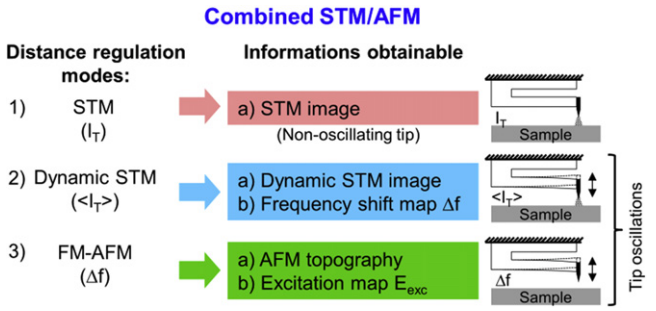

Figure 2. Imaging modes of a combined STM/AFM microscope based on a qPlus sensor: (1) STM mode, (2) dynamic STM and (3) FM-AFM.

microscopy (STM) [3–25]. During the growth of graphene on 6H–SiC(0001) surface due to sublimation of Si atoms from the SiC surface, the EG was found to cover a complex SiC precursor layer (here after called the buffer layer) which appears on the 6H–SiC(0001) substrate surface. For the morphology of the surface, STM images of EG monolayer covering the 6H–SiC(0001) $(6\sqrt{3} \times 6\sqrt{3})$ R30° reconstruction (referred as buffer layer in the remaining text) exhibit the carbon honeycomb lattice resting on the periodic corrugations of the underlying substrate. This regular arrangement of bumps can be described by a (6 × 6) quasi-cell with a 1.9 nm lattice period [5–8].

Besides these STM investigations, a few high resolution atomic force microscopy (AFM) studies of EG on 6H–SiC (0001) surface have been reported [22–25]. Filleter and Bennewitz by using an AFM working in non-contact mode in ultra-high vacuum (UHV) have observed a hexagonal lattice with a 1.9 nm period identified with the (6 × 6) quasi-cell but the operating conditions were not reported [22].

The corrugated surface of EG covering the buffer layer is reproduced in *ab initio* density functional theory (DFT) studies of Varchon *et al* [12] and Kim *et al* [13]. In both studies, the distance between the graphene and the buffer layer is found to be modulated along the [11] direction of the (6 × 6) quasi-cell. The structure of graphene monolayer on top of the reconstructed buffer layer on 6H–SiC(0001) surface is displayed in side view model in figure 1. The model shows that the graphene layer follows the atomic structure of the buffer layer underneath it and presents a lower surface corrugation, with respect to the buffer layer ($C_G < C_{BL}$). Also, no covalent bond is visible between the buffer layer and the graphene monolayer, they are weakly interacting via type van der Waals forces. In contrast, the buffer layer is covalently bound to the top most silicon atoms of the 6H–SiC(0001) substrate [9, 12, 13, 26] as observed. The figure 1(c) in [13] shows the position of carbon atoms with covalent $\sigma-$bonding to surface silicon atoms and the of $\pi-$orbitals region in the buffer layer. Considering the presence of this modulated distance and the well-known graphite distortion induced by the STM tip [27], we wonder whether the STM and AFM tips could induce any distortion during observations of EG on the reconstructed 6H–SiC(0001) surface.

Here, we present a study of the structure and mechanical properties of EG on a 6H–SiC(0001) $(6\sqrt{3} \times 6\sqrt{3})$ R30° reconstructed surface by using a combined scanning tunneling microscope/frequency modulated atomic force microscope (STM/FM-AFM) platform based on a qPlus sensor, working in UHV at room temperature. With an oscillating tip, dynamic STM and AFM images obtained on this surface together with two dimensional maps of force-gradient variation and energy dissipation, respectively, indicates some mechanical interaction between the tip and the EG covering the 6H–SiC(0001) surface. Finally, we discuss the consequences of this interaction on the observed morphology of EG with scanning probe microscopes.

2. Experimental

The 6H–SiC(0001) samples from NovaSiC were first chemically cleaned including trichloroethylene, acetone, and methanol in an ultrasonic bath. Then the sample was immediately introduced into a quartz glass reactor and heated under pure Ar (pressure 1 bar) at 1550 °C for 15 min following the process reported in [15]. After this treatment, the samples were transferred in air to the STM/AFM chamber. Once in the UHV chamber (base pressure 5×10^{-10} mbar) of the STM/AFM microscope, the samples were heated at (500–600)°C for 1 h to remove the contamination due to atmosphere exposure, and cooled down to room temperature before observations.

The combined STM/AFM system used in this study has been previously described [28]. Briefly, it consists in a modified variable-temperature UHV Omicron microscope working at room temperature coupled to a homemade preamplifier which is connected to a NANONIS-SPECS controller. A quartz tuning fork (Citizen American CFS206, $f_0 = 32\ 768$ Hz), glued in a qPlus geometry onto an Omicron holder equipped with a tip electro-etched from a Pt/Ir wire or a carbon fiber is the self-sensing probe. The scanning probe microscope was driven following three modes of tip/sample distance regulation (figure 2). In the first mode (1), the Z distance between the non-oscillating tip and the sample is adjusted to keep constant the tunneling current intensity (I_T) (standard STM operation mode). In the other regulation modes (2,3), a feedback loop adjusts the excitation signal E_{exc} of qPlus sensor for maintaining constant the oscillation amplitude of the tip above the surface. In the so-called dynamic STM mode (2), a feedback loop regulates the mean

Z distance between the oscillating tip and the sample to keep constant the mean tunneling current ($\langle I_T \rangle$). Simultaneously with dynamic STM images, a map is recorded reproducing the variations of the frequency shift related to changes in force gradients between the tip and sample (Δf map for the considered tunneling conditions). In the last mode of regulation (3), AFM topography of the surface is obtained in frequency modulation mode (FM-AFM) when the feedback loop adjusts the mean Z distance in order to keep constant the frequency shift (Δf) of the resonant probe. In the same time, another map can be recorded which reproduces the variations of the excitation signal E_{exc} [29]. Therefore, due to these additional information obtained simultaneously, as maps of Δf for dynamic STM mode and maps of E_{exc} for FM-AFM mode, the combined STM/FM-AFM microscope allows a better understanding of the mechanical properties of materials to sub-nanometric scale.

We mainly used STM/AFM tips electrochemically etched in a $CaCl_2$ solution from a 50 μm diameter Pt/Ir wire and carefully rinsed in hot deionized water. Then each tip was installed in a devoted UHV chamber to determine its apex radius from Fowler–Nordheim plots after removing possible residual contamination by high electric field desorption [30]. Only tips with an apex radius below 10 nm are glued on the free prong of a qPlus probe. Typically, the oscillation amplitude of the Pt/Ir tip was set between 0.10 and 0.15 nm and the resonance frequency is around 30 kHz, while the Q factor of qPlus probe ranges typically between 1200 and 4500. The tip oscillation amplitude was calibrated via the thermally induced Brownian motion [31]. The product of the high spring constant ($k \sim 8333$ N m^{-1}) of the tuning fork by its small oscillation amplitude is large enough to avoid jump-to-contact.

The combined STM/AFM measurements with Pt/Ir tips were only achieved with a positive Δf which corresponds to a repulsive regime between the tip apex and the graphene surface. As some insulating contamination at the apex on a few tips may be present, and influence the imaging conditions, we have carried out several observations by using tips electrochemically etched from carbon fiber. With such carbon fiber tip exempted from insulating compound [32], the same repulsive regime was observed when a tunneling current was detected. The force gradient that the tip undergoes during the STM regulation was calculated using the relation proposed by Giessibl for small oscillation amplitudes of the tip [33]. Finally, measurements of E_{exc} modulation in FM-AFM studies can be used to build two-dimensional maps of energy dissipation between tip and surface [34, 35]. All the data were processed using either WSxM [36] or Gwyddion [37] software.

3. Results

The EG on reconstructed 6H–SiC(0001) surface was first observed using the STM working in constant current regulation mode with a non-oscillating Pt/Ir tip. This STM image (shown in figure 3) corresponds to the structures previously reported [5, 8] and shows up two lattices. The first one corresponds to a honeycomb contrast with a measured 0.24 nm period corresponding to a graphene monolayer. The other one, which modulates the apparent height of the graphene layer with a long range period, is identified with the $(6\sqrt{3} \times 6\sqrt{3})$R30° reconstruction of the underlying substrate. This structure can also be described as a quasi-periodic arrangement of bumps with a lattice period of 1.9 nm corresponding to a (6 × 6) quasi-cell. The measured surface corrugation for these experimental conditions is 62 pm.

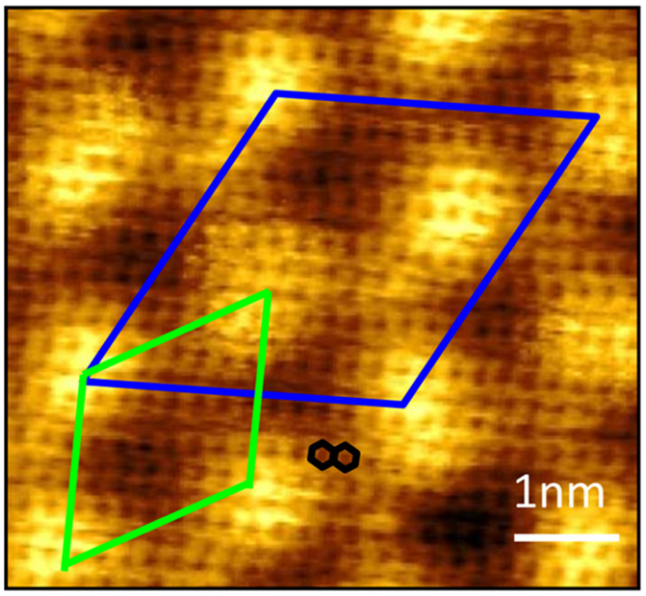

Figure 3. Constant current STM image of epitaxial graphene on the 6H–SiC(0001) $(6\sqrt{3} \times 6\sqrt{3})$R30° reconstructed surface (blue diamond) obtained with a non-oscillating Pt/Ir tip. The green diamond indicates the (6 × 6) quasi-cell of the underlying reconstructed SiC surface. The arrangement of small hollows with 0.24 nm period indicates the graphene lattice underlined by black hexagons. For STM: $V_T = -50$ mV, $I_T = 300$ pA.

Then, the structural, mechanical and electronic properties of this surface were explored with the STM/AFM platform using oscillating tips. Working with a Z-regulation based on the mean tunneling current; dynamic STM image and different maps were simultaneously recorded with different negative bias voltage values for EG on reconstructed 6H–SiC (0001) surface. Figure 4 displays a typical dynamic STM image obtained with regulation conditions keeping constant the mean tunneling current ($\langle I_T \rangle = 40$ pA) together with map of force-gradient variation. This dynamic STM image, which appears very similar to the one obtained in figure 3, presents bumps organized in a hexagonal lattice with a 1.9 nm period identified as the (6 × 6) quasi-cell. The measured height of bumps is 68 pm, a value agree to the height obtained in normal STM operations (figure 3) [6, 12, 14, 20] . We notice that the STM tip was in repulsive interaction with the surface since positive Δf values were measured as shown in figure 4(b). Such an interaction has been pointed out in AFM observations by optical beam deflection combined with measurements of tunneling current on graphite surface [38]. Remarkably the Δf map shown in figure 4(b) exhibits a

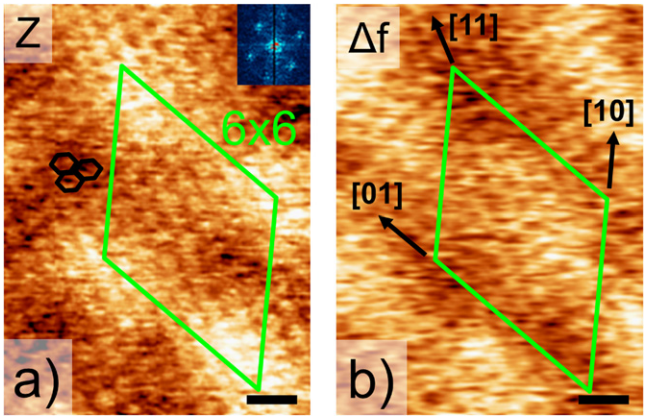

Figure 4. (a) Dynamic STM image obtained with an oscillating tip of an epitaxial graphene on a reconstructed 6H–SiC(0001) surface. The inset gives the FFT of the image, in which the hexagonal pattern correspond to the graphene lattice (black hexagons). (b) Associated maps of the frequency shift recorded during the image (a). ($V_T = -0.2$ V, $\langle I_T \rangle = 40$ pA, $A = 0.15$ nm, Z range is 100 pm, Δf range is 41–47 Hz). The green diamonds located in the same place underline the (6 × 6) quasi-cell. The black scale bar is 0.5 nm.

similar hexagonal lattice with a 1.9 nm period which is then attributed to the (6 × 6) quasi-cell. For these images, the values of tip/surface force gradient were found to range between 22.0 and 25.5 N m^{-1}. Considering the dynamic STM images obtained with different tips in this study, we notice that the associated mean force gradient had always positive value and varied between 2 and 40 N m^{-1} depending on the tunneling conditions and probably on the shape of the tip apex. The amplitude of the force gradient modulation along the [11] direction was found to vary in a limited range 1.5 N m^{-1} up to 6.0 N m^{-1}. Thus, these images bring evidence that EG on reconstructed 6H–SiC(0001) experienced a positive force gradient induced by the STM tip, whose position above the surface was regulated in the dynamic STM mode ($\langle I_T \rangle$ constant). There are two contributions in this force gradient, one is roughly constant and associated to the tunneling conditions while the other presents modulations related with the (6 × 6) quasi-cell. We also remark that the bumps in the dynamic STM image do not overlap the maxima in the frequency shift map as illustrated by the (6 × 6) quasi-cell located on the same place in each image of figure 4. Finally, we notice that the atomic lattice of EG is observed in the dynamic STM image (See the fast Fourier transform in the inset of figure 4(a) while a modulation with the same period (0.24 nm) is detected in the Δf map.

Switching to FM-AFM operation, Z-regulation of the oscillating tip is now based on keeping constant the shifted resonance frequency. Let us first present two AFM images obtained on the same surface with the same Pt/Ir tip for two different values of the setpoint: $\Delta f = +15$ and +20 Hz. Figure 5 presents the topographic images together with cross section profiles. From comparison with figure 3, the lattice of bumps with a 1.9 nm period is related to the (6 × 6) quasi-cell of EG covering the buffer layer. The relief amplitude in AFM topographies is found to depend on the setpoint value since it

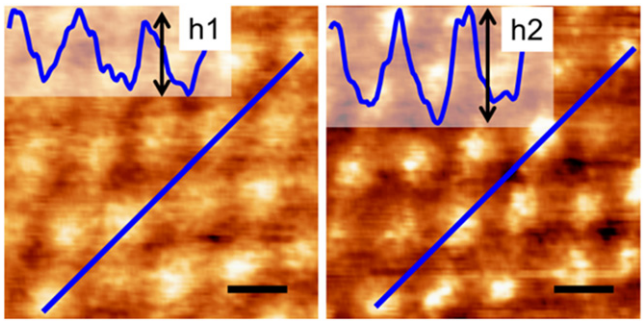

Figure 5. FM-AFM topography of epitaxial graphene on 6H–SiC (0001) obtained with a constant frequency shift equal to +15 Hz (left) and +20 Hz (right). The blues lines correspond to the profile sections shown in the top inset. The measured relief amplitudes ($h1$ and $h2$) are 60 and 88 pm. The black scale bar is 2 nm. (FM-AFM regulation: $A = 0.13$ nm, $V_T = -5$ mV).

increases from 60 to 88 pm for $\Delta f = +15$ and +20 Hz corresponding respectively to force gradient setpoints equal to 8 and 11 N m^{-1}. Therefore the measured relief amplitude of the (6 × 6) quasi-cell is clearly related to the intensity of the tip/surface interaction demonstrating that the AFM tip deforms EG on reconstructed 6H–SiC(0001), neglecting distortions of the Pt/Ir.

Figure 6 presents the AFM topography of the surface obtained for a setpoint $\Delta f = +20$ Hz with the corresponding E_{exc} map and the cross section profiles along the [11] direction of the (6 × 6) quasi-cell. Each image shows a periodic arrangement of bumps with 1.9 nm parameter associated with the (6 × 6) quasi-cell and the FFT of both images shows out a pattern of dots arranged hexagonally that confirm the (6 × 6) lattice. We point out that the topographic bumps correspond to minima of excitation energy as shown by the black arrows in both images. The comparison of cross section profiles along the same [11] direction demonstrate the non-overlapping of topography maxima with the ones of the E_{exc} map. Such a non-overlapping characterizes the EG on reconstructed 6H–SiC(0001) surface and is not a measurement artifact because the root mean square of deviations of the frequency shift due to noise of the feedback regulation is only 0.15 Hz. We also notice that the E_{exc} maxima (dashed red lines, see figure 6(d) are typically located between the topographic bumps along the [11] direction. As for the probe, coupled with the surface, was oscillating at its resonance frequency in these FM-AFM observations, contributions of conservative and dissipative forces in the tip/surface interaction can be separated [35]. In these conditions we can extract the variation of the dissipation in the tip/surface interaction from the E_{exc} map. Thus, the dissipated energy per cycle E_d is related to the excitation signal E_{exc} by the following expression:

$$E_d = \pi\, k\, A_0^2/Q \left[E_{exc}/E_{exc0} - f/f_0 \right], \qquad (1)$$

where E_{exc0} and f_0 are the excitation signal and the free resonance frequency without any tip/surface interaction, E_{exc} and f are the excitation signal and the resonance frequency with the tip interacting with the surface while Q and A_0 are the

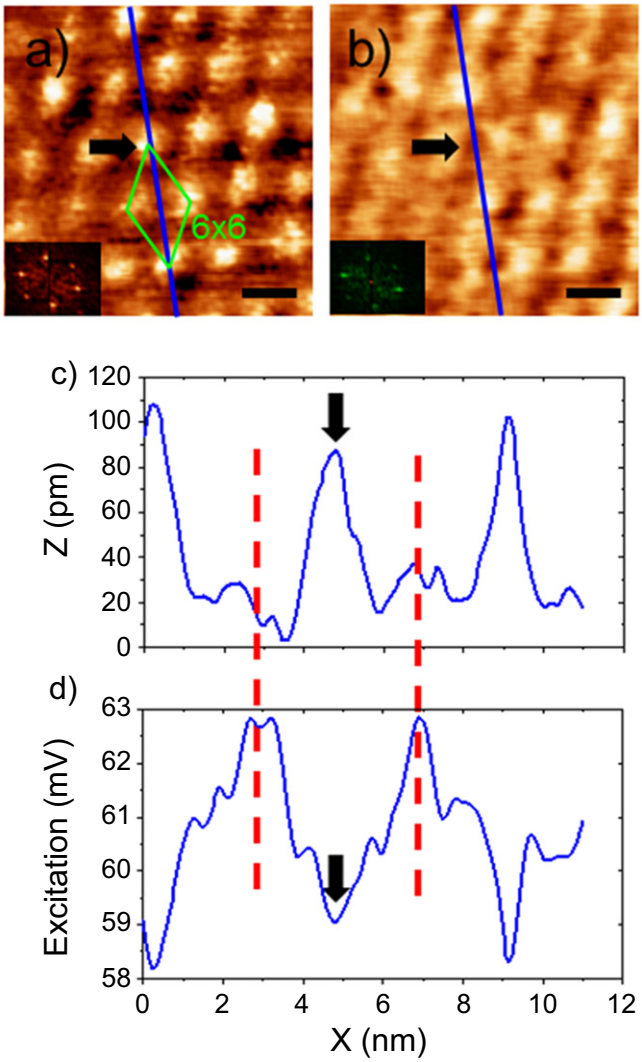

Figure 6. (a) FM-AFM topographic image with $\Delta f = +20$ Hz together with (b) simultaneously recorded maps of excitation signal. The black scale bar is Znm. The cross section profiles along the same [11] direction of the lattice are reported for each image in (c) and (d). Z range is 130 pm, Excitation signal range is 57–64 mV.

quality factor and the oscillating amplitude of the non-interacting tip, respectively. The values of energy dissipation extracted from the excitation map in figure 6(d) range from 1.32 to 1.65 eV/cycle. As a consequence, the tip/surface dissipation undergoes a periodic modulation equal to 330 meV/cycle when the FM-AFM tip scans in repulsive interaction over EG along the [11] direction of the (6 × 6) quasi-cell. Furthermore, such a dissipation modulation depends on the setpoint value since we have measured 190 and 330 meV/cycle for a setpoint equal to 15 and 20 Hz, respectively.

In the following part, the discussion will be focused on the mechanical distortion of EG during STM/AFM imaging and on the origin of this distortion. From several images obtained in dynamic STM mode with different tunneling conditions and different tips, the mean tip/surface force gradient can be found between 2 and 40 N m^{-1}. Such values correspond well to the setpoint values used for recording the AFM topographies shown in figures 5 and 6. Considering that the relief, measured in AFM images, depends on the setpoint for values around (5–15) N m^{-1}, we deduce that the graphene suffers mechanical distortions during dynamic STM studies. Any insulating compound at the Pt/Ir tip apex, which could mechanically couple the tip to the graphene, is excluded for two reasons. The first one is that figures 4 and 6 which show similar images were recorded with different Pt/Ir tips. The second reason is that similar STM images were observed with a tip etched from a carbon fiber (not shown here). Such detailed analyses of experimental data led us to conclude that the tip/surface interaction distorts STM images of EG on 6H–SiC(0001) recorded at constant current.

What is the origin of the EG distortion caused by the tip? We propose that the tip-induced EG distortion results from the conjunction of the electronic properties of graphene and its packing on the reconstructed 6H–SiC(0001) surface. It is well known that the weak local density of states (LDOS) of graphite/graphene [39, 40] forces the STM tip to be close to the surface. In fact, the deformation of a graphite surface induced by a STM tip was proposed more than twenty years ago in order to explain giant corrugation in STM images of this material [27] and confirmed by AFM measurements [38]. Furthermore, elastic properties of a graphene monolayer are now well known from distortion of free standing graphene membrane by AFM nanoindentation [41]. The other origin of the observed distortions is related to the packing of graphene on a reconstructed 6H–SiC(0001) surface. Let us first consider the periodic variation of the tip-induced distortions observed in figure 6. It indicates that local mechanical properties of the graphene are modulated by the underlying corrugated substrate. This is supported by the amplitude of energy dissipation modulations measured in FM-AFM images which ranges from 190 to 330 meV/cycle for a setpoint increasing from 15 to 20 Hz. As these dissipation changes appear higher than the ones measured with the same instrument on polythiophene molecules on graphite (75 meV/cycle) [28], they could involve distortions of a notable part of EG covering one (6 × 6) quasi-cell. Taking in account the hardness of a SiC crystal, spatial modulations of the mechanical distortion of EG and energy dissipation are probably connected to changes in the distance between the graphene and the substrate within the (6 × 6) quasi-cell. The DFT calculations of Varchon *et al* [12] have shown that the (6 × 6) corrugation of the buffer layer topography is rather large with a height difference close to 120 pm while the EG relief amplitude induced by the underlying structure is only 40 pm. Thus, the variation of the distance between the graphene and the buffer layer reaches 80 pm in these calculations. We emphasize that such a variation corresponds to a 24% deviation of the graphite inter-plane distance (0.335 nm). Similar distance modulations were reported in another study based on DFT calculations [13]. As the calculated distance between the graphene and the buffer layer in-between the (6 × 6) bumps is larger than the graphite interplanar distance, tip-induced EG distortion would be favored in between the bumps of the buffer layer and by the tip/surface interaction. As a consequence both the increasing relief amplitude

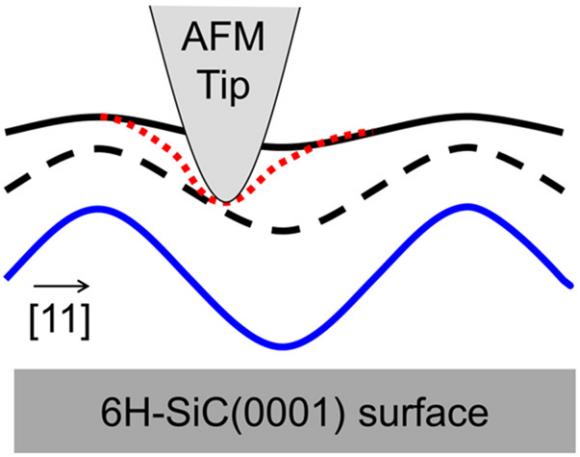

Figure 7. Schematic view of the AFM tip induced distortion of the epitaxial graphene on reconstructed 6H–SiC(0001) surface along the [11] direction of the (6 × 6) quasi-cell. The blue line is for the buffer layer, the solid black one represents the epitaxial graphene layer and the dashed line is for the trajectory of the tip end in repulsive mode. The red dotted line corresponds to the graphene locally distorted by the tip.

depending on the Δf values and the larger dissipation values measured in between the topographical bumps strongly support EG distortions induced by the tip. The scheme shown in figure 7 illustrates how the AFM tip (or STM tip) working in repulsive mode induces local distortions of the graphene on reconstructed 6H–SiC(0001) surface.

Other examples of tip-induced distortions of graphene layers have been pointed out at different scales and for several substrates. Recently atomic resolution was achieved with a qPlus probe in air on quasi-freestanding monolayer graphene on 6H–SiC(0001) for a large frequency shift (456 Hz up to 600 Hz) [42]. In another example, some observed lateral displacements of graphene ridges on 6H–SiC(0001) terraces had been related to strong STM tip/surface interaction [43]. Analysis of STM images of graphene resting on SiO_2 substrate [44] and also the ones of non-supported graphene membrane [45] led to the conclusion of tip induced distortions of graphene layers. Recently, another example of tip-induced graphene distortion has been evidenced for EG on Ru(0001) for a tip in attractive mode [46]. For EG on Ir(111), a good agreement between experimental data and DFT calculations was reported [47] suggesting low tip-induced distortion. For this system, the force gradient of 2.21 N m^{-1} (repulsive regime) measured by Dedkov *et al* [48, 49] during constant height AFM experiments is ten times smaller than the force gradient reported here. Such a force gradient (typically 20 N m^{-1}) was required for measuring a tunneling current, which is probably related to the smaller LDOS of EG on 6H–SiC(0001) than the one of EG on Ir (111).

4. Conclusion

In summary, the structural and mechanical properties of EG monolayers on 6H–SiC(0001) were studied by using a combined STM/AFM system based on a qPlus probe working in UHV. This scanning probe platform, equipped with a Pt/Ir tip, was operated at room temperature under different modes of regulation. The AFM topography and STM image of EG layer exhibit a periodic lattice of protrusions identified with the (6 × 6) quasi-cell related to the underlying reconstruction of the 6H–SiC(0001) surface. In addition, the maps of frequency shift or excitation variations, simultaneously recorded, show up modulations with the same lattice. Furthermore, the amplitude of the (6 × 6) quasi-cell corrugation in AFM topography increases with the setpoint value of the frequency shift. From analysis of all the images it turns out the following conclusion. During imaging, the AFM or STM tip induces a variable mechanical distortion of EG on reconstructed 6H–SiC(0001) surface. Such a modulated distortion demonstrates that the distance between the EG and the underlying substrate varies along [11] direction of the (6 × 6) quasi-cell. Such a variable distance agrees well with the results obtained by two DFT calculations [12, 13]. These findings are of general importance for a deep understanding of properties of EG covering a 6H–SiC(0001) $(6\sqrt{3} \times 6\sqrt{3})R30°$ reconstructed surface. In particular, the consequences of these tip-induced distortions of graphene covering this substrate in the contrast of STM images deserve new studies.

Acknowledgments

The authors wish to thank Y Dappe, S Latil, (CEA/IRAMIS/SPEC/GMT) for fruitful discussions about the electronic properties of epitaxial graphene on 6H–SiC(0001) surface. A Ouerghi ((CNRS-LPN), Route de Nozay, 91460 Marcoussis, France) who kindly provided the epitaxial graphene samples is gratefully thanked as well as L Pham-Van and J Polesel-Maris (CEA/IRAMIS/SPEC) for discussions on AFM measurements.

José Antonio Morán Meza would also like to acknowledge financial support from Réseau Thématique de Recherche Avancée (RTRA-Triangle de la Physique) and CEA/Direction des Relations Internationales (DRI).

References

[1] Geim A K and Novoselov K S 2007 The rise of graphene *Nat. Mater.* **6** 183–91
[2] Wintterlin J and Bocquet M-L 2009 Graphene on metal surfaces *Surf. Sci.* **603** 1841–52
[3] Berger C *et al* 2004 Ultrathin epitaxial graphite: 2D electron gas properties and a route toward graphene-based nanoelectronics *J. Phys. Chem.* B **108** 19912–6
[4] Chen W *et al* 2005 Atomic structure of the 6H–SiC(0001) nanomesh *Surf. Sci.* **596** 176–86
[5] Riedl C, Starke U, Bernhardt J, Franke M and Heinz K 2007 Structural properties of the graphene-SiC(0001) interface as a key for the preparation of homogeneous large-terrace graphene surfaces *Phys. Rev.* B **76** 245406
[6] Brar V W *et al* 2007 Scanning tunneling spectroscopy of inhomogeneous electronic structure in monolayer and bilayer graphene on SiC *Appl. Phys. Lett.* **91** 122102

[7] Rutter G M *et al* 2007 Imaging the interface of epitaxial graphene with silicon carbide via scanning tunneling microscopy *Phys. Rev.* B **76** 235416

[8] Mallet P, Varchon F, Naud C, Magaud L, Berger C and Veuillen J-Y 2007 Electron states of mono- and bi-layer graphene on SiC probed by scanning-tunneling microscopy *Phys. Rev.* B **76** 041403

[9] Mattausch A and Pankratov O 2007 *Ab Initio* study of graphene on SiC *Phys. Rev. Lett.* **99** 076802

[10] Virojanadara C, Syväjarvi M, Yakimova R, Johansson L, Zakharov A and Balasubramanian T 2008 Homogeneous large-area graphene layer growth on 6H–SiC(0001) *Phys. Rev.* B **78** 245403

[11] Emtsev K V, Speck F, Seyller T, Ley L and Riley J D 2008 Interaction, growth, and ordering of epitaxial graphene on SiC{0001} surfaces: a comparative photoelectron spectroscopy study *Phys. Rev.* B **77** 155303

[12] Varchon F, Mallet P, Veuillen J-Y and Magaud L 2008 Ripples in epitaxial graphene on the Si-terminated SiC(0001) surface *Phys. Rev.* B **77** 235412

[13] Kim S, Ihm J, Choi H and Son Y-W 2008 Origin of anomalous electronic structures of epitaxial graphene on silicon carbide *Phys. Rev. Lett.* **100** 176802

[14] Lauffer P, Emtsev K V, Graupner R, Seyller T and Ley L 2008 Atomic and electronic structure of few-layer graphene on SiC(0001) studied with scanning tunneling microscopy and spectroscopy *Phys. Rev.* B **77** 155426

[15] Emtsev K V *et al* 2009 Towards wafer-size graphene layers by atmospheric pressure graphitization of silicon carbide *Nat. Mater.* **8** 203–7

[16] Starke U and Riedl C 2009 Epitaxial graphene on SiC (0001) and SiC (000-1): from surface reconstructions to carbon electronics *J. Phys.: Condens. Matter* **21** 134016

[17] Riedl C, Coletti C and Starke U 2010 Structural and electronic properties of epitaxial graphene on SiC(0001): a review of growth, characterization, transfer doping and hydrogen intercalation *J. Phys. D: Appl. Phys.* **43** 374009

[18] Qi Y, Rhim S H, Sun G F, Weinert M and Li L 2010 Epitaxial Graphene on SiC (0001): more than just honeycombs *Phys. Rev. Lett.* **105** 085502

[19] Forti S, Emtsev K V, Coletti C, Zakharov A A, Riedl C and Starke U 2011 Large-area homogeneous quasifree standing epitaxial graphene on SiC(0001): electronic and structural characterization *Phys. Rev.* B **84** 125449

[20] Choi J, Lee H and Kim S 2010 Atomic-scale investigation of epitaxial graphene grown on 6H–SiC (0001) using scanning tunneling microscopy and spectroscopy *J. Phys. Chem.* C **114** 13344–8

[21] Goler S *et al* 2013 Revealing the atomic structure of the buffer layer between SiC(0001) and epitaxial graphene *Carbon, NY* **51** 249–54

[22] Filleter T and Bennewitz R 2010 Structural and frictional properties of graphene films on SiC(0001) studied by atomic force microscopy *Phys. Rev.* B **81** 155412

[23] Castanié F, Nony L, Gauthier S and Bouju X 2012 Graphite, graphene on SiC, and graphene nanoribbons: calculated images with a numerical FM-AFM *Beilstein J. Nanotechnol.* **3** 301–11

[24] Boneschanscher M P, van der Lit J, Sun Z, Swart I, Liljeroth P and Vanmaekelbergh D 2012 Quantitative atomic resolution force imaging on epitaxial graphene with reactive and nonreactive AFM probes *ACS Nano* **6** 10216–21

[25] Held C, Seyller T and Bennewitz R 2012 Quantitative multichannel NC-AFM data analysis of graphene growth on SiC (0001) *Beilstein J. Nanotechnol.* **3** 179–85

[26] Varchon F *et al* 2007 Electronic structure of epitaxial graphene layers on SiC: effect of the substrate *Phys. Rev. Lett.* **99** 126805

[27] Soler J M, Baro A M, Garcia N and Rohrer H 1986 Interatomic forces in scanning tunneling microscopy: giant corrugations of the graphite surface *Phys. Rev. Lett.* **57** 444–7

[28] Polesel-Maris J, Lubin C, Thoyer F and Cousty J 2011 Combined dynamic scanning tunneling microscopy and frequency modulation atomic force microscopy investigations on polythiophene chains on graphite with a tuning fork sensor *J. Appl. Phys.* **109** 074320

[29] Morán Meza J A 2013 Propriétés structurelles et électroniques du graphène sur SiC (0001) étudiées par microscopie combinée STM/AFM *PhD Thesis* Université Paris Sud 11 (France)/Université Nationale d'Ingénierie de Lima (Peru)

[30] Morán Meza J A *et al* 2015 Reverse electrochemical etching method for fabricating ultra-sharp platinum/iridium tips for combined scanning tunneling microscope/atomic force microscope based on a quartz tuning fork, (unpublished manuscript)

[31] Giessibl F J 2000 Atomic resolution on Si(111)-(7 × 7) by noncontact atomic force microscopy with a force sensor based on a quartz tuning fork *Appl. Phys. Lett.* **76** 1470–2

[32] Castellanos-Gomez A, Agraït N and Rubio-Bollinger G 2010 Carbon fibre tips for scanning probe microscopy based on quartz tuning fork force sensors *Nanotechnology* **21** 145702

[33] Giessibl F J 2003 Advances in atomic force microscopy *Rev. Mod. Phys.* **75** 949–83

[34] Gotsmann B, Seidel C, Anczykowski B and Fuchs H 1999 Conservative and dissipative tip–sample interaction forces probed with dynamic AFM *Phys. Rev.* B **60** 51–61

[35] Farrell A *et al* 2005 Conservative and dissipative force imaging of switchable rotaxanes with frequency-modulation atomic force microscopy *Phys. Rev.* B **72** 125430

[36] Horcas I, Fernández R, Gómez-Rodríguez J M, Colchero J, Gómez-Herrero J and Baro A M 2007 WSXM: a software for scanning probe microscopy and a tool for nanotechnology *Rev. Sci. Instrum.* **78** 013705

[37] Nečas D and Klapetek P 2011 Gwyddion: an open-source software for SPM data analysis *Cent. Eur. J. Phys.* **10** 181–8

[38] Kawai S and Kawakatsu H 2009 Surface-relaxation-induced giant corrugation on graphite (0001) *Phys. Rev.* B **79** 115440

[39] Wallace P R 1947 The band theory of graphite *Phys. Rev.* **71** 622–34

[40] Dappe Y J, González C and Cuevas J C 2014 Carbon tips for all-carbon single-molecule electronics *Nanoscale* **6** 6953–8

[41] Lee C, Wei X, Kysar J W and Hone J 2008 Measurement of the elastic properties and intrinsic strength of monolayer graphene *Science* **321** 385–8

[42] Wastl D S, Weymouth A J and Giessibl F J 2014 Atomically resolved graphitic surfaces in air by atomic force microscopy *ACS Nano* **8** 5233–9

[43] Sun G F, Jia J F, Xue Q K and Li L 2009 Atomic-scale imaging and manipulation of ridges on epitaxial graphene on 6H–SiC(0001) *Nanotechnology* **20** 355701

[44] Stolyarova E *et al* 2008 Scanning tunneling microscope studies of ultrathin graphitic (graphene) films on an insulating substrate under ambient conditions *J. Phys. Chem.* C **112** 6681–8

[45] Klimov N N *et al* 2012 Electromechanical properties of graphene drumheads *Science* **336** 1557–61

[46] Koch S *et al* 2013 Elastic response of graphene nanodomes *ACS Nano* **7** 2927–34

[47] Altenburg S J and Berndt R 2014 Local work function and STM tip-induced distortion of graphene on Ir(111) *New J. Phys.* **16** 053036

[48] Dedkov Y S *et al* 2013 Electronic structure and imaging contrast of graphene moiré on metals *Sci. Rep.* **3** 1072

[49] Dedkov Y, Voloshina E and Fonin M 2015 Scanning probe microscopy and spectroscopy of graphene on metals *Phys. Status Solidi* **252** 451–68